Supporting information

Janus fabric sensor with integrated moisture-wicking, wearable monitoring and thermoelectric system for fire-warning

Kai Yan [a]*, Jun Wang [a], Yan Zong [a], Qunna Xu [a], Fei Xu [b], Tongtong Wang [b]

[a] College of Bioresources Chemical and Materials Engineering, Shaanxi University of Science & Technology, Xi'an 710021, PR China

[b] College of Advanced Materials Engineering, Jiaxing key Laboratory of Preparation and Application of Advanced Materials for Energy Conservation and Emission Reduction, Jiaxing Nanhu University, Jiaxing, Zhejiang 314001, PR China

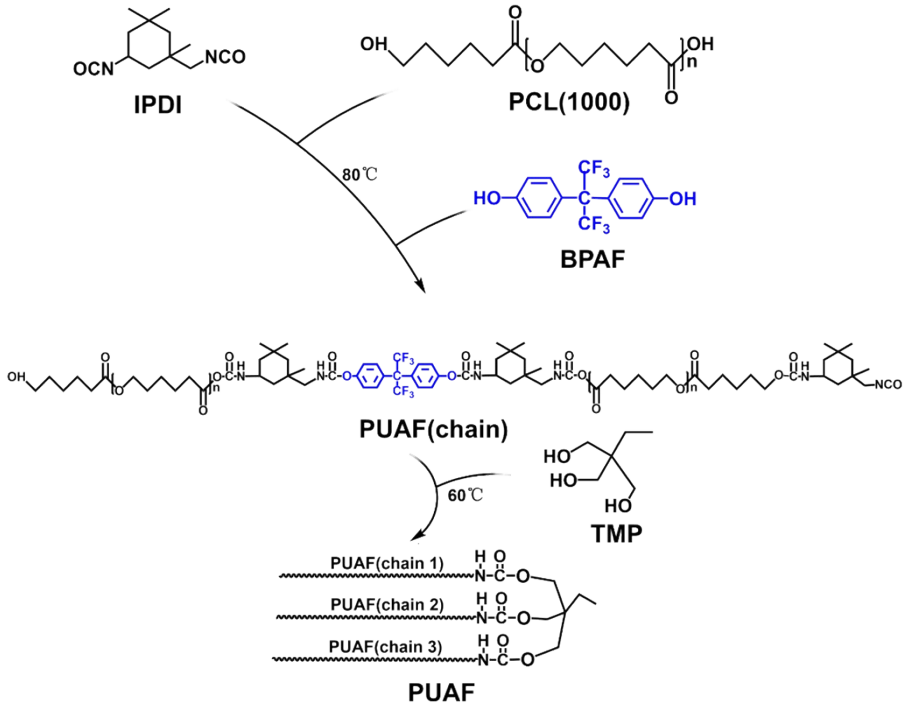

Fig. S1 Schematic diagram for the preparation of PUAF.

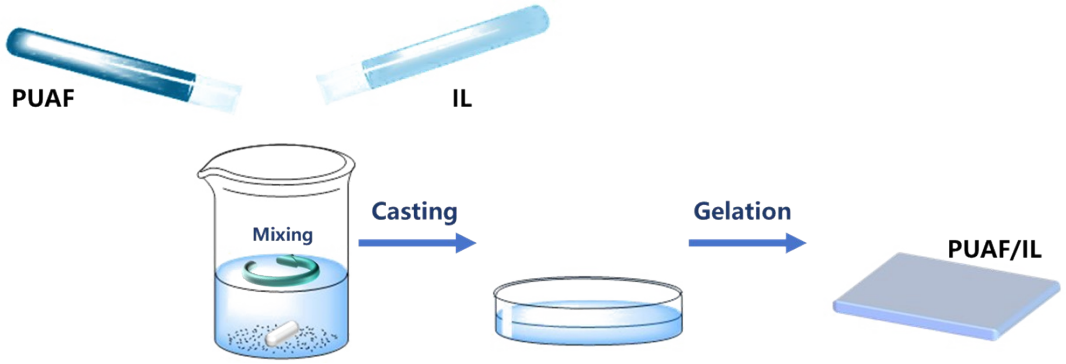

Fig. S2 Diagram illustrating PUAF/IL gelation.

The FT-IR spectra of the pristine fabric and PPy fabric was presented in Fig. S3. In the spectrum of the pristine fabric, a broad characteristic peak at 3320 cm^{-1} is observed, corresponding to the O-H group of cellulose. For the PPy fabric, a peak at 1232 cm^{-1}, attributed to the C-N stretching vibration, confirming the successful in-situ polymerization of PPy on the cellulose structure of the fabric.

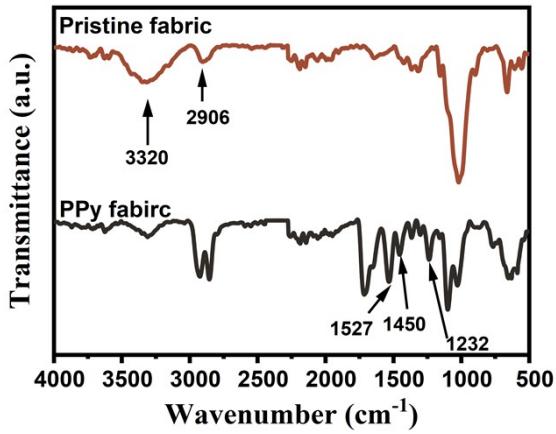

Fig. S3 FT-IR spectra of pristine fabric and PPy fabric.

The cross-sectional SEM image of the Janus fabric sensor is presented in Fig. 4a, revealing its asymmetric architecture with a hydrophilic upper surface and a hydrophobic lower surface. The surface morphologies of the two sides exhibited distinct characteristics in terms of fiber density and texture (Fig. 4b-c). The hydrophilic side displays relatively loose fiber arrangement with minimal polymer coating, whereas the hydrophobic side shows densely packed and interconnected fibers with more extensive polymer coverage.

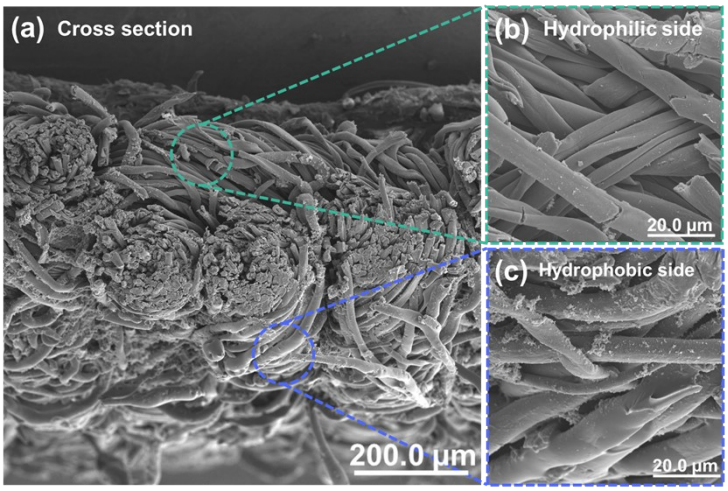

Fig. S4 SEM image of a) cross section, b) hydrophilic side and c) hydrophobic side of JF-3.5. Scale bar 200.0 µm and 20.0 µm.

The mechanical durability of the Janus fabrics was systematically evaluated through sandpaper abrasion testing on both surfaces. As shown in Fig. S7a, under a 10g load and 10 cm reciprocating stroke length, the hydrophobic side was subjected to varying cycles of abrasion (10, 20, 30, 40, and 50 cycles). The water pumping time through the hydrophobic side exhibited negligible deterioration after repeated abrasion. Specifically, the pumping time increased by only 1.5s after 50 cycles compared to 10 cycles. Similarly, the hydrophilic side was tested under same conditions (Fig. S7b), and the pumping time remained consistent across all abrasion cycles (10-50 cycles). These results showed that both surface coatings of the Janus fabric possess sufficient adhesion strength to withstand typical daily usage.

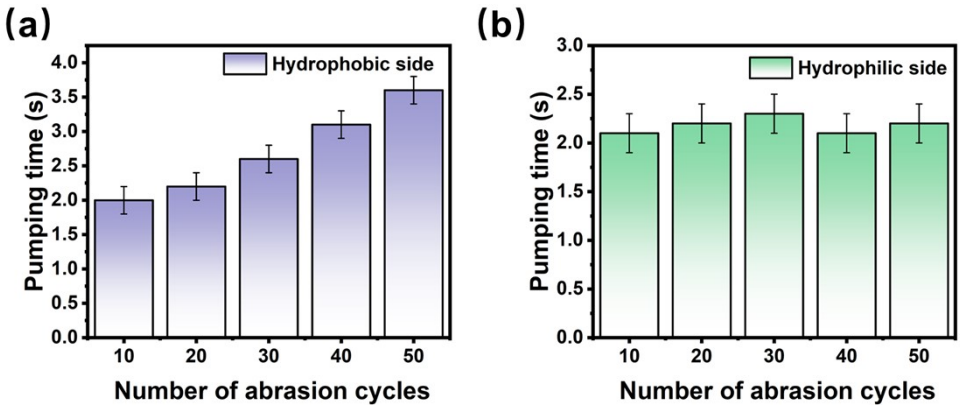

Fig. S5 Water pumping time in the JF-3.5 after (a) abrasion cycles on the hydrophobic side and (b) abrasion cycles on the hydrophilic side: 10, 20, 30, 40, and 50 cycles.

According to the standards of GB/T 12704 and GB/T 5453, the air permeability of pristine and JF-3.5 was assessed using the air permeability tester (YG(B)461D, Darong Textile Instrument, China) and moisture permeability tester (YG(B)216G, Darong Textile Instrument, China). As shown in Fig. S6, the average air permeability for the pristine fabric was 86.33 mm/s, whereas the fabric demonstrated a lower permeability with an average value of 63.65 mm/s. Notably, the average water vapor permeability increased from 1674 to 1839 g/m²/24h. It still was suitable for personal wear.

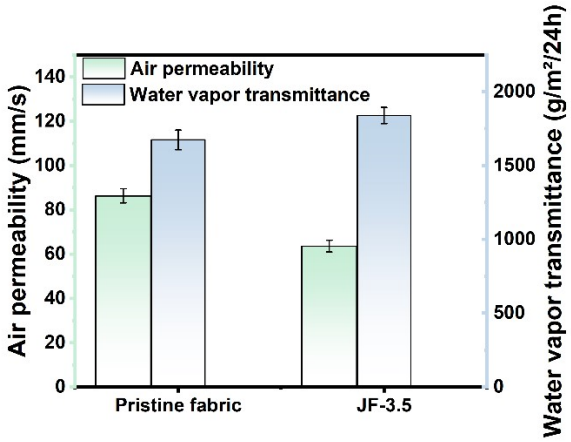

Fig. S6 Air permeability and water vapor transmittance of the pristine fabric and JF-3.5.

As shown in Fig. S7, the experimental results indicated that the fastest unidirectional water transport achieved its minimum time of 2s when the PUAF/IL loading content was optimized at 3.5 wt%. Water transport was accomplished with a pumping time of 6 seconds when the loading was 4.0 wt%. However, water transport was inhibited when the loading exceeded 3.5 wt%. This inhibition is likely due to excessive coating material blocking the capillary channels responsible for water transport.

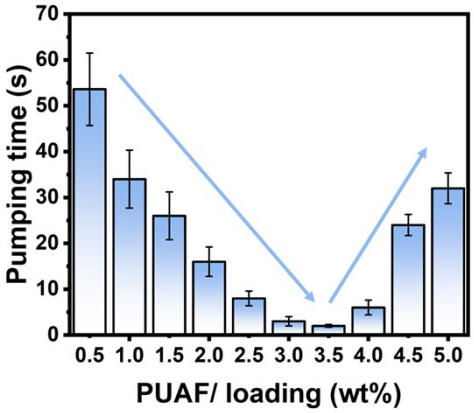

Fig. S7 Water pumping time in the Janus fabrics at different PUAF/IL loading.

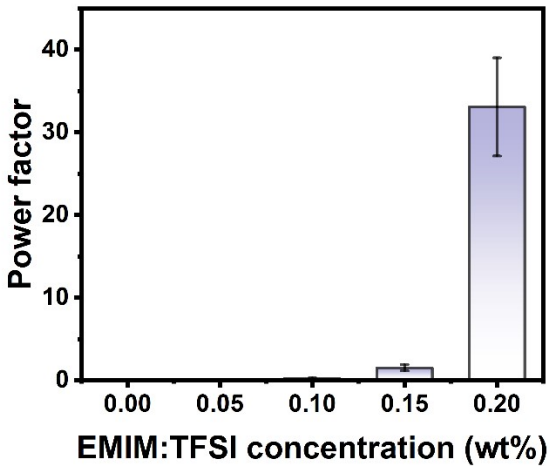

Fig. S8 Power factor of PUAF/IL i-TE gels prepared with different EMIM:TFSI weight ratios.

The thermal conductivity (κ) of different samples was presented in Figure S9. The PUAF/IL i-TE gel exhibited the highest thermal conductivity of 0.320 $W \cdot m^{-1} \cdot K^{-1}$. When incorporated into the Janus fabric sensors, the overall thermal conductivity of the Janus fabric sensor remained generally low due to its relatively low concentration. Specifically, the thermal conductivity increased from 0.036 $W \cdot m^{-1} \cdot K^{-1}$ at 0.5 wt% loading to 0.057 $W \cdot m^{-1} \cdot K^{-1}$ at 3.5 wt% loading.

The influence of thermal conductivity on the temperature difference and output voltage of thermoelectric devices can be quantitatively evaluated through the dimensionless figure of merit ZT_i, which is defined as:

$$ZT_i = \frac{S^2 \sigma T}{\kappa}$$

where S represents the Seebeck coefficient (V/K), σ denotes the electrical conductivity (S/m), T is the absolute operating temperature (K), and κ represents the thermal conductivity ($W \cdot m^{-1} \cdot K^{-1}$). The Seebeck coefficient and calculated ZT_i values of the Janus fabric samples are summarized in Table 1. The results indicated that while the thermal conductivity (κ) of the Janus fabric sensors showed a slight increase, the Seebeck coefficient (S) primarily exhibited a positive correlation with the loading content of PUAF/IL i-TE. Notably, the impact of thermal conductivity on the figure of merit ZT_i of the Janus fabric sensors was relatively minor.

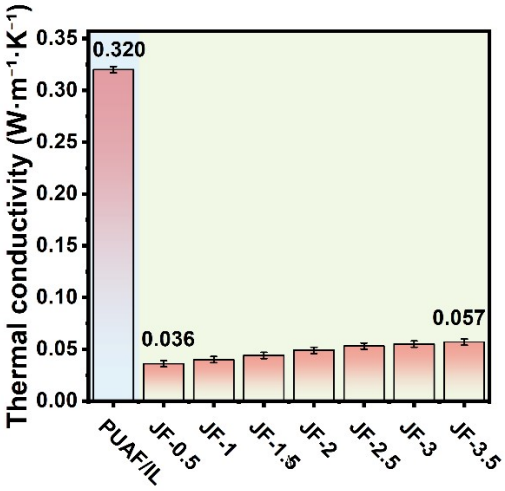

Fig. S9 Thermal conductivity of PUAF/IL i-TE gel and different Janus fabric sensors.

The influence of sweat on strain sensing and thermoelectric performance was investigated. As shown in Fig. S10a, during the cycle tests, artificial sweat solution was periodically introduced, and the relative resistance changes ($\Delta R/R_0$) were recorded at different artificial sweat conditions. It can be seen that the $\Delta R/R_0$ decreased gradually under the same strain. Compared to the resistance at 0 wt% artificial sweat loading, the resistance at 100 wt% increased by 31%. It provided a calibration reference for R_0 in strain sensing at different sweat conditions. Notably, when testing at the same strain and frequency under different artificial sweat concentration, the strain sensing signals showed a negligible difference. Strain sensing results are presented at 0, 20, 40, 60, 80 and 100 wt% artificial sweat concentration (Fig. S10c-h). Under the same strain, the peak $\Delta R/R_0$ of the JF-3.5 varied by less than 3% within a 20 wt% sweat condition.

Furthermore, to observe thermoelectric trend intuitively, thermoelectric measurements was conducted under specific sweat conditions (Fig. S10b). Interestingly, under the condition of increased artificial sweat concentration, the thermoelectric voltage of the Janus fabric sensor showed a slight increase, from an initial 4.84 mV/K to 5.35 mV/K at 100 wt% artificial sweat concentration. This could be due to the sweat facilitating the ion diffusion in the i-TE gel. Demonstrating that the Janus fabric sensor can perform accurate and reliable strain sensing and thermoelectric response at various sweat conditions.

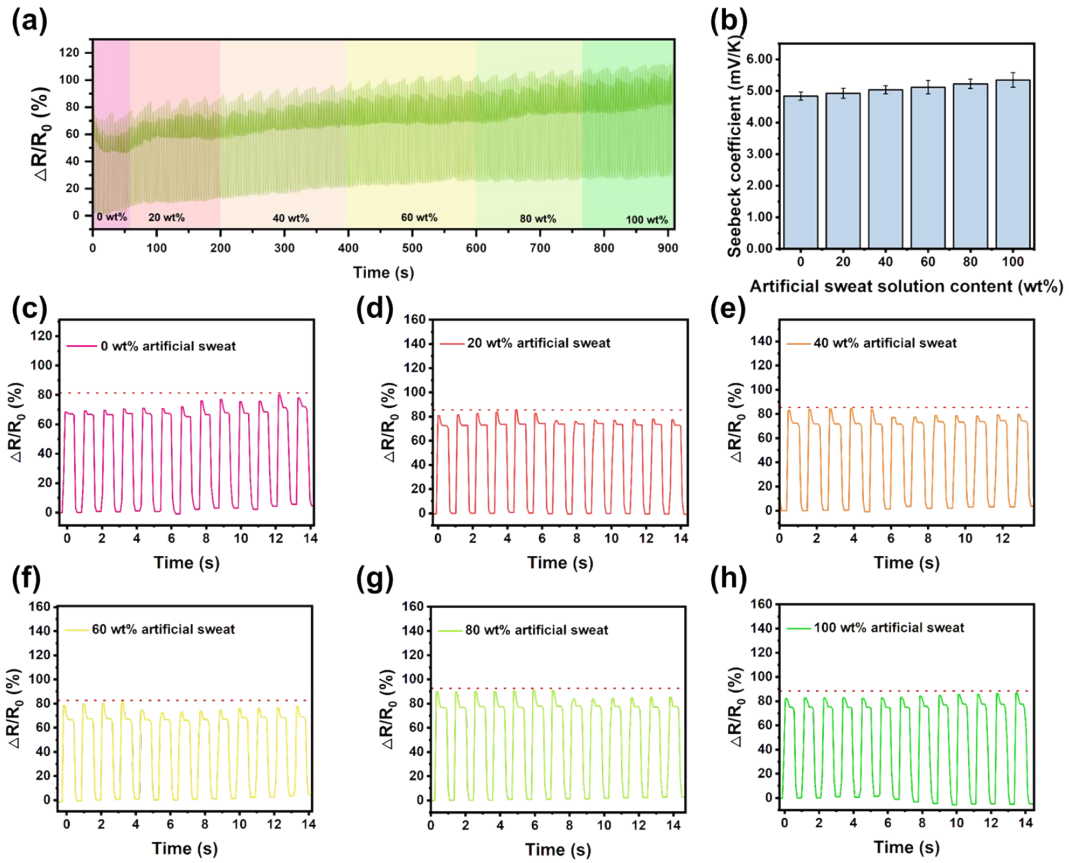

Fig. S10 (a) $\Delta R/R_0$ curves of the JF-3.5 during cycling tests with continuous introduction of artificial sweat. (b) Seebeck coefficient of the JF-3.5 under different artificial sweat conditions. $\Delta R/R_0$ curves of the JF-3.5 under 10% strain cyclic tests at different artificial sweat conditions:(c) 0 wt%, (d) 20 wt%, (e) 40 wt%, (f) 60 wt%, (g)80 wt% and (h) 100 wt%.

Table S1 The Seebeck coefficient and calculated ZT_i values of the Janus fabric samples

Samples	Seebeck coefficient (V/K)	ZT_i
JF-0.5	3.31×10^{-3}	0.891
JF-1	3.56×10^{-3}	0.882
JF-1.5	3.62×10^{-3}	0.898
JF-2	3.84×10^{-3}	0.843
JF-2.5	3.97×10^{-3}	0.824
JF-3	4.69×10^{-3}	0.963
JF-3.5	4.83×10^{-3}	0.959